Manuscript prepared for Atmos. Chem. Phys. Discuss.
with version 4.0 of the LaTeX class copernicus_discussions.cls.
Date: 4 February 2015

Stratospheric and mesospheric HO_2 observations from the Aura Microwave Limb Sounder

L. Millán[1,2], S. Wang[2], N. Livesey[2], D. Kinnison[3], H. Sagawa[4], and Y. Kasai[4]

[1]Joint Institute for Regional Earth System Science and Engineering, University of California, Los Angeles, California, USA
[2]Jet Propulsion Laboratory, California Institute of Technology, Pasadena, California, USA
[3]National Center for Atmospheric Research, Boulder, Colorado, USA
[4]National Institute of Information and Communications Technology, Koganei, Tokyo, Japan

Correspondence to: L. Millán (lmillan@jpl.nasa.gov)

Abstract

This study introduces stratospheric and mesospheric hydroperoxyl radical (HO_2) estimates from the Aura Microwave Limb Sounder (MLS) using an offline retrieval (i.e. run separately from the standard MLS algorithm). This new dataset provides two daily zonal averages, one during daytime and one during nighttime, with a varying vertical resolution from about 4 km at 10 hPa to around 14 km at 0.0032 hPa. A description of the methodology and an error analysis are presented. Comparisons against the Whole Atmosphere Community Climate Model (WACCM), the Superconducting Submillimeter-Wave Limb-Emission Sounder (SMILES) and the Far Infrared Spectrometer (FIRS-2) measurements, as well as, photochemical simulations demonstrate the robustness of the retrieval and indicate that the retrieval is sensitive enough to detect mesospheric HO_2 layers during both day and night. This new dataset is the first long-term HO_2 stratospheric and mesospheric satellite record and it provides needed constraints to help resolve the O_3 deficit problem and the "HO_x dilemma".

1 Introduction

Since 1985, when for the first time the now famous O_3 hole was reported (Farman et al., 1985), the stratospheric O_3 layer has received massive scientific attention. Although it peaks in the lower stratosphere, this layer extends well into the mesosphere where O_3 chemistry is controlled by catalytic cycles involving the HO_x (HO_2, OH and H) family (Brasseur and Solomon, 2005)

$$X + O_3 \rightarrow XO + O_2 \quad \text{(R1)}$$

$$O + XO \rightarrow O_2 + X \quad \text{(R2)}$$

where the net effect of these two reactions is simply,

$$O + O_3 \rightarrow 2O_2 \quad \text{(R3)}$$

which destroys O_3 without changing the abundance of the catalyst, X, which in this case is either OH or H.

The presence of the HO_x family in the middle atmosphere is a consequence of the transport of H_2O and CH_4 from the troposphere to higher altitudes. The production of HO_x species in the middle atmosphere is primarily due to O_3 photolysis

$$O_3 + h\nu \rightarrow O_2 + O(^1D) \quad \text{(R4)}$$

$$O(^1D) + H_2O \rightarrow 2OH \quad \text{(R5)}$$

$$OH + O_3 \rightarrow O_2 + HO_2 \quad \text{(R6)}$$

and, above 60 km, by photodissociation of H_2O by absorption of UV radiation (particularly in the Lyman–Alpha region and the Schumann–Runge bands),

$$H_2O + h\nu \rightarrow OH + H \quad \text{(R7)}$$

where H turns into HO_2 due to the three body reaction

$$H + O_2 + M \rightarrow HO_2 + M \quad \text{(R8)}$$

The removal of HO_x is mainly through the self-reaction,

$$HO_2 + OH \rightarrow H_2O + O_2 \quad \text{(R9)}$$

and the partitioning between OH and HO_2 above ~ 40 km is primarily driven by,

$$HO_2 + O \rightarrow OH + O_2 \quad \text{(R10)}$$

$$H + O_3 \rightarrow O_2 + OH \quad \text{(R11)}$$

$$OH + O \rightarrow O_2 + H \quad \text{(R12)}$$

where the H produced in Reaction (R12) is quickly converted to HO_2 by Reaction (R8).

Despite the apparent simplicity of the HO_x chemistry, models were not able to give a complete picture of its chemistry in the middle atmosphere: Summers et al. (1997) reported that OH satellite observations by the Middle Atmosphere High Resolution Spectrograph Investigation (MAHRSI) were 30 to 40 % lower than the values computed using standard photochemical models. Sandor et al. (1998) reported that mesospheric

ground based microwave measurements of HO_2 were 23 to 47 % higher than photochemical model predictions at midday, agreed with the model values prior to 9 a.m. LT, and were 70 to 100 % higher immediately after sunset. Jucks et al. (1998) using simultaneous OH and HO_2 balloon observations by the Far Infrared Spectrometer (FIRS-2) reported that OH agreed reasonably well with model estimates, a conclusion supported by Pickett et al. (2008), while HO_2 was 25 % higher than the model estimates. However, Canty et al. (2006) concluded that, at least between 25–60 km, the HO_x Microwave Limb Sounder (MLS) and FIRS-2 observations were reasonably well described by photochemical models. In addition to these modeling discrepancies, a problem known as the HO_x dilemma, models have consistently under-predicted the amounts of O_3 at such altitudes, an issue known as the O_3 deficit problem (Crutzen and Schmailzl, 1983; Solomon et al., 1983; Eluszkiewicz and Allen, 1993; Summers et al., 1997; Varandas, 2004; Siskind et al., 2013).

There have been many suggested solutions for the "HO_x dilemma" and the O_3 deficit problem in the literature (e.g. Miller et al., 1994; Jucks et al., 1998; Varandas, 2004); however, difficulties persist, in part, because there are very few observations of HO_2 in the mesosphere. To date, there are four mesospheric datasets available: (1) six days spread between April 1992 and December 1996 measured by the Kitt Peak National Radio Astronomy Observatory (NRAO) (Sandor et al., 1998), (2) the Sub-Millimeter Radiometer (SMR) aboard the Odin satellite dataset (Baron et al., 2009), which consists of one observation period of 24 h each month between October 2003 and December 2005, (3) the Superconducting Submillimeter-Wave Limb-Emission Sounder (SMILES) dataset (Kikuchi et al., 2010), which provides daily coverage from 38° S to 65° N between October 2009 and April 2010, and (4) the standard MLS dataset (Pickett et al., 2006, 2008), which provides coverage mostly from 55° S to 55° N, up to 0.046 hPa and only during daytime.

In this study, we introduce a new dataset of global observations of stratospheric and mesospheric HO_2 from the MLS instrument. This new offline (i.e. run separately from the standard MLS algorithm) retrieval extends the HO_2 vertical range well into the

mesosphere (up to 0.003 hPa or ~ 90 km), which, in addition to the standard MLS H_2O, OH and O_3, potentially allows the MLS dataset to study the HO_x–O_3 chemical system to provide insights for the long-standing O_3 deficit problem. To date, this dataset provides ten years of data and, in the near future, it will be publicly available for download in a daily based hierarchical data format (HDF). In the next section we give an overview of the MLS instrument as well as the MLS HO_2 measurements. Section 3 presents the offline retrieval approach and describes its vertical resolution, precision, and systematic uncertainties. Comparisons between the offline MLS HO_2 dataset and global climate model simulations, balloon-borne and satellite datasets are shown in Sect. 4. Lastly, the offline HO_2 data are compared to the results of a 1-D photochemical model to investigate if standard reaction rates can model the extended HO_2 vertical range. Section 5 provides a summary.

2 MLS HO_2 observations

The Microwave Limb Sounder (MLS) is, in essence, a small radio telescope on board the Aura satellite which was launched into a polar sun-synchronous orbit in July 2004. MLS measures limb millimeter and submillimeter atmospheric thermal emission at 120 different tangent altitudes from the ground to about 95 km every 24.7 s. It covers latitudes between 82° S and 82° N, providing near global observations with roughly half of these measurements during daytime (~ 13:45 LT), and the other half during nighttime (~ 1:45 LT), except near the poles where the observations transition between daytime and nighttime conditions and vice-versa. The incoming radiance is collected by a 1.6 m antenna which directs it onto four heterodyne radiometers covering spectral regions near 118, 191, 240, and 640 GHz (a fifth radiometer located at 2.5 THz is fed by a separate antenna). The radiant flux measured by the GHz radiometers is then analyzed by 22 filter banks and 4 digital autocorrelator spectrometers. Most of these filter banks were designed to measure essentially a single spectral line, despite the doubleside band nature of the radiometers (i.e. each filter bank measures two different spectral

regions, one on each side of the local oscillator). Furthermore, these banks have narrower filters at the band center than at the extremes allowing them to measure the strong pressure broadening at microwave frequencies. A more detailed description of the Aura MLS instrument is given by Waters et al. (1999) and Waters et al. (2006).

HO_2 is measured by two of these filter banks, known as band 28 and band 30, centered at the 649.72 and 660.50 GHz HO_2 lines. These filter banks consist of 11 channels with widths varying from 6 to 32 MHz, giving a total width of around 200 MHz. An example of the observed radiances is shown in Fig. 1. The ~ 1 K HO_2 signal is relatively small compared to the individual limb radiance precision which varies from 2 K at the bands edges to 4 K at the band center (gray dotted line), hence some averaging is required to obtain HO_2 abundances with a useful signal to noise ratio. The clear tilt in band 30 is due to the proximity of an O_3 line.

As mentioned above, HO_2 is one of the MLS products retrieved with the standard algorithm described in Livesey et al. (2006a). Briefly, the algorithm uses the optimal estimation technique (Rodgers, 2000) retrieving one profile for each scan using a two-dimensional approach. The smallness of the HO_2 signal translates to a retrieved product usable only between 10 and 0.046 hPa. For greater pressures, the signal is lost due to pressure broadening (i.e. Fig. 1 shows how the lines broaden rapidly as the pressure increases) and stronger emissions from O_3. For smaller pressures the signal is indistinguishable from the noise.

The latest version (V3.3) of the MLS HO_2 standard product (Pickett et al., 2008; Livesey et al., 2011) produces ~ 3500 abundance profiles daily with typical precisions varying from 0.15 ppbv (52×10^6 cm^{-3}) at 10 hPa to 3 ppbv (5×10^6 cm^{-3}) at 0.046 hPa for measurements zonally averaged and binned in a 10° latitude bin. Due to the seasonality of HO_2, these values can change up to 10 % depending on the pressure level observed. Its vertical resolution varies from 4 to 10 km between 10 and 0.046 hPa. In this pressure range, since negligible HO_2 is expected at night ($\sim$ 1:45 a.m. LT for MLS at the equator), it is recommended to use the non-zero nighttime abundances as an indication of systematic biases (i.e. affecting both day and night retrievals). Hence,

the HO_2 day–night difference should be used as a better estimate of the daytime HO_2 than taking the daytime measurements at face value. During summer and winter, this restricts the usable HO_2 standard product data to between roughly 55° S and 55° N, where MLS observes both daytime and nighttime data. In addition to the MLS HO_2 product, this day–night difference approach to ameliorate biases has been used successfully for the BrO and OH MLS products (Livesey et al., 2006b; Pickett et al., 2008; Millán et al., 2012).

3 Offline retrieval

For this study, an HO_2 offline retrieval has been developed similar to that described by Millán et al. (2012). In essence, we compute a daily zonal mean of the radiances, for band 28 and 30, from which we retrieve daily HO_2 concentrations. The daily zonal mean radiances are formed by collocating them into 10° latitude bins, sorting them into daytime and nighttime using solar zenith angles (SZAs) lower than 90° and greater than 100°. Those radiances having SZAs in between 90° and 100° are disregarded to avoid twilight measurements. These sorted radiances are then averaged onto a vertical grid with six pressure levels per decade (spacing of ~ 3 km) using the tangent pressure retrieved by the standard algorithm.

The retrieval uses the optimal estimation technique as described by Rodgers (2000) assuming an HO_2 a priori of zero, an a priori precision of 20 ppbv and using the corresponding daily zonal means of temperature, O_3, HNO_3, and HCl from the standard MLS algorithm (version 3.3) as part of the atmospheric state. In addition to this constraint, a Twomey–Tikhonov regularization (Tikhonov, 1963; Twomey, 1963) is used to reduce noise and smooth the profiles at the expense of some vertical resolution. Furthermore, at each pressure level, a constant baseline is retrieved for each band to correct any instrument baselines as well as to take care of the water vapor continuum contribution. The best retrievals were found when doing a joint band 28 and 30 retrieval

as opposed to doing retrievals using only band 28 or only band 30, even despite the O_3 line influencing band 30.

The offline daytime HO_2 estimates are confined to a pressure range between 10 and 0.0032 hPa with day–night differences used as a measure of daytime HO_2 for pressures between 10 and 1 hPa where the nighttime values exhibit non-zero values indicative of biases. Note that, a visual inspection of the 10^o bin monthly average profiles has shown, overall, no sings of a discontinuity at 1 hPa when using this approach. The offline nighttime HO_2 estimates are confined to a pressure range between 1 and 0.0032 hPa.

Figure 2 shows monthly (January 2005) zonal means for the standard and offline HO_2 datasets in volume mixing ratio (VMR) and density units. The temperature used to convert the data from VMR to number density is the same zonal mean temperature from the standard MLS algorithm that is used as part of the atmospheric state. As can be seen, the offline retrieval has two distinct improvements over the standard product: (1) an extended pressure range, which enables the measurements of the mesospheric local maxima that occur at around 0.02 hPa at most latitudes, and (2) an extended latitudinal coverage, allowing to measure the polar regions, where in the summer one, the HO_2 maximum lies. Furthermore, as shown in the following sections, it also estimates HO_2 during night. Note that the standard MLS product is smoother because it is highly constrained due to the poor signal to noise ratio of the individual radiance profiles.

3.1 Vertical resolution

Figure 3 shows typical averaging kernels for the HO_2 offline retrieval. These kernels delimitate the region of the atmosphere from which the information is contributing to the retrieved values at a given pressure level. As such, their full width at half maximum (FWHM) is a measure of the vertical resolution. The offline HO_2 product has a vertical resolution of about 4 km between 10 and 0.1 hPa, 8 km at 0.02 hPa and around 14 km for smaller pressures. The vertical resolution of this offline retrieval is similar to that of the HO_2 standard product for the pressure range where they overlap. The integrated kernel shows that most of the information arises from the measurements.

3.2 Error assessment

The total error in the retrieved product is a combination of the random noise in the measurements, the smoothing error, and the errors due to systematic uncertainties, such as instrumental and calibration errors and forward model and retrieval approximations.

Figure 4 displays the offline HO_2 expected precision for daily, monthly, and yearly profiles of measurements averaged over a 10° latitude bin. The expected precision is the error due to the combination of the random noise in the measurements and the a priori uncertainty and is given by the diagonal elements of the covariance matrix of the retrieved state (Rodgers, 2000). For measurements averaged over a 10° latitude bin, for both the daytime and nighttime data, the daily HO_2 precision ranges from 0.09 ppbv (29×10^6 molec cm^{-3}) at 10 hPa to 1.4 ppbv (2.2×10^6 molec cm^{-3}) at 0.046 hPa, and up to 7.7 ppbv (1×10^6 molec cm^{-3}) at 0.003 hPa. Due to the temporal variability of HO_2, these precision values can change seasonally up to 40 % depending on the pressure level observed. This variability is greater than the one found in the standard MLS product because the standard product is highly constrained due to the poor signal to noise ratio. Although significant averaging such as monthly means is needed to achieve usable HO_2 estimates, the retrieval algorithm presented in this study uses daily zonal mean radiances, instead of weekly or monthly, in order to enable averaging different combination of days as needed.

Figure 5 summarizes the impact of the dominant systematic uncertainties for the offline MLS HO_2 product. These arise from instrumental issues such as uncertainties in the radiometric calibration, the Field of View (FOV) characterization, the spectroscopy parameters, the pointing knowledge, the temperature profile used, the contaminant species errors, such as the O_3 line influencing band 30, and the retrieval approximations (a complete list and a more detailed discussion of the systematic error analysis is given by Read et al., 2007, Appendix A). The contribution of these uncertainties to the total HO_2 error was estimated using end-to-end calculations. For each systematic error a full day (~ 3500 profiles) of perturbed radiances was generated and binned into

10° zonal bins and processed by the offline algorithm. Each perturbation corresponds to either 2σ estimates of uncertainties in the relevant parameter, or an estimate of their maximum reasonable error based on instrument knowledge. Comparisons of these results with those using unperturbed radiances are a measure of the impact of each systematic error source. The comparison between the unperturbed noise-free radiances run, and the "true" model atmosphere estimates the errors due to the retrieval numerics, which, in other words, is a measure of error due to the retrieval formulation itself, in this case, mostly an smoothing error.

The impact of typically small error sources, such as (but not limited to) errors due to the spectrometer nonlinearities, uncertainties in the MLS spectral filter position, and the antenna transmission losses, has been quantified with a simple analytical model of the MLS measurement system (Read et al., 2007, Auxiliary material). Unlike the end-to-end estimates, these calculations only provide a multiplicative error.

Between 10 and 0.1 hPa, both for the daytime and nighttime case, the total systematic error is around 0.04 ppbv (up to $\sim 10 \times 10^6$ molec cm^{-3}). In this region, the main source of systematic bias arises from radiometric and spectroscopy uncertainties, in particular due to standing waves. Standing waves are a consequence of multiple reflections in the MLS optics of the hot and cold targets used as part of the radiometric calibration (Jarnot et al., 2006). For pressures smaller than 0.1 hPa, the main source of bias and scatter are retrieval numerics, which, although unsatisfactory, is understandable given the ~ 14 km vertical resolution in this region. Around 0.0032 hPa, the total error is as large as 1.2 ppbv ($\sim 0.2 \times 10^6$ molec cm^{-3}) .

4 Results

In this section we compare the offline HO_2 dataset with balloon-borne and other satellite measurements, as well as with global climate and photochemical model simulations. In making these comparisons, i.e. when showing the absolute or percentage differences between the datasets, the MLS averaging kernels has been applied to

properly compare them. Furthermore, when comparing the global climate or the photochemical model simulations, their high vertical resolution has been reduced to the MLS one using a least square fit as described by Livesey et al. (2011, Sect. 1.9). In these comparisons, no altitude extrapolation has been applied to any dataset. To alleviate biases in the MLS offline HO_2 data, the daytime–nighttime differences are used as a measure of daytime HO_2 for pressures between 10 and 1 hPa.

4.1 Comparison with balloon-borne instruments

Figure 6 compares the MLS offline and the Far Infrared Spectrometer (FIRS-2) HO_2 data. The MLS HO_2 profile corresponds to daytime–nighttime differences averaged over a 20° latitude bin centered at 30° N averaged over 10 days centered on the day of the balloon flight. The mean SZA of this profile is $\sim 32°$. The FIRS-2 profile shown was taken on the 20 September 2005 in Fort Sumner, New Mexico, USA (34.5° N). In that flight, the balloon stayed aloft at around 38 km for nearly 24 h. The FIRS-2 profile with the closest SZA to the MLS one is displayed, in this case $\sim 31°$.

FIRS-2 is a thermal emission far-infrared Fourier transform spectrometer developed at the Smithsonian Astrophysical Observatory. It measures emission spectra between 75 and 1000 cm^{-1} with high interferometric efficiency. It retrieves HO_2 from 43 rotational transitions between 110 and 220 cm^{-1} (Jucks et al., 1998). The retrieval algorithm first estimates slant columns and then, in an onion-peeling fashion, a singular value decomposition routine is used to retrieve mixing ratios on a 1 km vertical grid (Johnson et al., 1996). The total systematic errors for the retrieved HO_2 are estimated to be 3 %.

Overall, the two instruments agree on the HO_2 vertical structure, with increasing HO_2 with height (in the VMR representation) however there seems to be an bias between them, with the MLS data in the lower bound. This might be due to the differences between the FIRS-2 single profile and the MLS zonal mean profile. In SD-WACCM (see Sect. 4.3 for the model description), these differences (i.e. comparing a single profile versus a zonal mean profile at this location) are around 30%. Quantitatively, the

MLS offline data agrees with the FIRS-2 data within their uncertainties. Result also found by Pickett et al. (2008) using the standard MLS HO_2 product.

4.2 Satellite intercomparison

Comparisons of monthly means were made with those from the Superconducting Submillimeter Wave Limb Emission Sounder (SMILES). SMILES is a 4 K cooled radiometer on board the Japanese Experiment Module (JEM) on the International Space Station (ISS) that performed atmospheric observations from October 2009 to April 2010. It measured, on a time sharing basis, two of three frequency bands: 624.32–625.52 GHz (band A), 625.12–626.32 GHz (band B), and 649.12–650.32 GHz (band C) covering tangent heights between 10 and at least 60 km about 1600 times per day covering mostly from 65° N to 38° S. HO_2 retrievals are based on radiances from band C which measures an HO_2 line centered at 649.7 GHz (the same line measured by the upper-side band of MLS band 28). The ISS follows a non-sun synchronized circular orbit with an inclination of 51.6° which allowed SMILES to make measurements at local times that drifted ~ 20 min earlier each day covering the entire diurnal cycle in a period of about 2 months (Kikuchi et al., 2010). In this study we use the HO_2 retrievals from the research processor (version 3.0.0) developed by NICT (National Institute of Information and Communications Technology). This version is an outcome of the latest calibrated radiances which includes an improved determination of the tangent height (e.g. Ochiai et al., 2013). These HO_2 retrievals have been used for inter-satellite comparisons (Khosravi et al., 2013) and for a reaction rate estimation (Kuribayashi et al., 2014). They have a vertical resolution varying from 4 to 5 km at 35 and 55 km, respectively. The estimated precision of a single profile was estimated to be better than 30 % in the vertical range 20–86 km. In this study, only retrieval levels with a measurement response greater than 0.8 and lower than 1.2 have been used to avoid altitudes influenced too much by the apriori (Baron et al., 2011).

Figures 7 and 8 show daytime and nighttime comparisons (monthly means and the differences of the monthly means), respectively. Note that only SMILES measurements

made within half an hour local time of the MLS measurements were used in this comparison. During daytime, the retrieval top level difference is as much as 80 %, however at around 0.02 hPa (the mesospheric local maxima height), the difference is overall less than $\pm 30\,\%$. The retrieval top level differences will need to be explored further, to investigate if they are due to retrieval artifacts (both retrievals are more sensitive to the apriori at these levels), calibration uncertainties or sampling differences (unlike MLS, SMILES data are not regularly distributed); this will require a joint effort from the MLS and SMILES teams. During nighttime, the overall differences are around 30 % with localized spikes due to the small nighttime values. Overall, below around 0.1 hPa these HO_2 estimates agree within their uncertainties.

Comparisons against SMR were not performed for two reasons: (1) the SMR mesospheric data mentioned in Sect. 1 are not publicly available and (2) SMR ascending and descending-node times are about 6.00 a.m. and 6.00 p.m., just during sunrise and sunset which complicates the comparison.

4.3 Comparison with a global climate model

The Whole Atmosphere Community Climate Model (WACCM Version 4) is a fully interactive chemistry climate model where the radiatively active gases affect heating and cooling rates and therefore dynamics (Garcia et al., 2007). It simulates the atmosphere from the Earth's surface to the thermosphere. For this analysis, the model was run with a horizontal resolution of $1.9^\circ \times 2.5^\circ$ in latitude and longitude, and a vertical coordinate purely isobaric in the stratosphere with a variable spacing of 1.1 to 1.75 km using meteorological fields derived from the Goddard Earth Observing System 5 (GEOS-5) analyzes. The use of offline meteorological fields, a capability described by Lamarque et al. (2012), allows WACCM to perform as a chemical transport model, thus facilitating comparisons with observations. The WACCM chemical module is based on the 3-D chemical transport Model of Ozone and Related Tracers (MOZART), Version 4 (Kinnison et al., 2007). The results of this Specified Dynamics WACCM (SD-WACCM/GEOS-5) run were then sampled to the corresponding MLS observation time.

Figure 9 shows a daytime monthly (January 2005) mean comparison between the offline MLS data and the SD-WACCM simulations both in VMR and density units. As can be seen, both display similar VMR structures with a gradient from the winter pole towards the summer pole. Note that to properly compare the data with the model simulations, Fig. 9 also shows the SD-WACCM simulations convolved with the offline MLS averaging kernels reducing the SD-WACCM high vertical resolution using a least square fit as described by Livesey et al. (2011, Sect. 1.9).

In Fig. 9, the HO_2 VMR peak between 0.05 and 0.01 hPa reflects the mesospheric source (Reaction R8 following Reaction R7). The latitudinal gradient is a consequence of the varying SZA and the H_2O distribution, which also shows a latitudinal gradient due to the meridional circulation. The height of this peak is set by the balance between the thin air density at higher altitudes and the weakening of the UV irradiance responsible for the H_2O photolysis at lower altitudes, which leads to smaller HO_2 production.

In the stratosphere, as H_2O photolysis becomes less important and the H abundance decreases, HO_2 mainly forms from the transformation of OH through reactions with O_3 (Reaction R6). This source is reflected in the HO_2 number density peak in the stratosphere and has a similar shape to the peak of OH (e.g., Pickett et al., 2008) but at lower altitudes due to the O_3 maximum height in the lower stratosphere.

Even though the offline MLS dataset and the SD-WACCM simulations display similar structures (see Fig. 9), they differ in magnitude. The offline MLS data suggest that there is more mesospheric HO_2 than predicted by the model, particularly at ~ 0.02 hPa, which requires further investigation. These differences correspond to SD-WACCM values smaller than the retrieved values by 50 % near the summer pole and smaller than 80 % near the winter pole (where SD-WACCM estimates near zero values).

To investigate if these discrepancies, particularly the ~ 4 ppbv difference at around 50° S, were due to measurement errors or due to assumptions in the SD-WACCM model, we compared measured MLS radiances to synthetic radiances computed using the offline MLS data and the SD-WACCM values. The SD-WACCM simulated radiances were smaller than the measured radiances by $\sim 40\,\%$, outside the radiance

error. Although MLS calibration errors cannot be ruled out, this is unlikely due to the magnitude of the offset and because this type of discrepancies cannot be found in the nighttime monthly mean comparison (Fig. 11). Hence, these simulations suggest that there is more mesospheric HO_2 than modeled at around 0.02 hPa. Furthermore, as can be seen in the latitude/time cross section shown in Fig. 10, the behavior found in Fig. 9 (a 50 % difference near the summer pole and more than 80 % near the winter one) repeats itself. These discrepancies might be due to a variety of reasons, for example: (1) our understanding of middle atmospheric chemistry may not be complete, (2) there might be due to differences between recent solar spectral irradiance (SSI) satellite measurements (Snow et al., 2005; Harder, 2010) and most parameterizations. These SSI measurements display a larger variability in solar UV irradiance which cannot be reconstructed with SSI models, including the model of Lean et al. (2005), used in this SD-WACCM run (Marsh et al., 2013). These SSI measurement-model differences have been proven to affect the HOx photochemistry (Haigh et al., 2010; Merkel et al., 2011; Ermolli et al., 2013); more UV irradiance leads to an enhancement of O3 photolysis as well as H_2O photodissociation, which leads to more HO_x production through (Reactions R4 to R8). Further, Wang et al. (2013) showed that using a solar forcing derived from these SSI measurements the modeled OH variability agrees much better with observations. Lastly, (3) these discrepancies might be related to the WACCM representation of the mean meridional circulation which has been shown to have some deficiencies (Smith et al., 2011; Smith, 2012), suggesting that the gravity wave parametrization needs to be modified. In addition, Garcia et al. (2014) has shown that adjusting the Prandtl number, used to calculate the diffusivity due to gravity waves, significantly alters the CO_2 SD-WACCM simulations improving its agreement with satellite measurements. Such adjustment should also affect the H_2O and hence the HO_x chemistry.

Figure 9 also shows that SD-WACCM underpredicts HO_2 by about 20–30% between 1 and 0.1 hPa. This result agrees with previous studies (Sandor et al., 1998; Khosravi et al., 2013) but contradicts the result of the study by Canty et al. (2006). The apparent

model overestimation near 0.2 hPa is probably related to the MLS change in vertical scan pattern near this pressure level.

In Fig. 9 in the number density subplots, between 10 and 0.1 hPa, both the offline MLS dataset and the SD-WACCM simulations behave in a similar manner both in structure and in magnitude; however, due to the small HO_2 signal in the MLS radiances, the offline MLS retrieval is noisier. The lack of a peak at $\sim$0.02 hPa in the SD-WACCM dataset reflects the smaller mesospheric concentrations in this dataset.

Figure 11 shows the nighttime monthly mean comparison. As in the daytime comparison, both datasets show similar structures with a narrower HO_2 layer in the upper mesosphere as well as a gradient from the winter to the summer pole. As during daytime, HO_2 is principally formed through the three-body reaction of H with O_2 (Reaction R8); however in this case, due to the lack of photodissociation of H_2O, the H available is the one generated at sunlit latitudes (in this case, in the northern hemisphere), transported at high altitudes towards the winter pole where it descends and reacts with O_2 at night (in this case, in the southern hemisphere) (Pickett et al., 2006). As in daytime, despite having similar structures, both datasets differ in magnitude. Overall, the nighttime differences are smaller than the daytime differences, with SD-WACCM underpredicting the midlatitude summer regions by as much as 30 % and overestimating by as much as 50 % over the polar winter regions.

The strong contrast, around 6 ppbv, between the daytime and the nighttime HO_2 mesospheric peaks demonstrates the capability of the new offline retrieval to invert large mesospheric variations.

4.4 Photochemical model comparisons

Figure 12 shows a comparison between the HO_2 estimates from MLS offline and model simulations using the Caltech/JPL-Kinetics 1-D photochemical model. This model covers from the surface to 130 km in 66 layers. It has vertical transport (including eddy, molecular and thermal diffusion) and coupled radiative transfer (Allen et al., 1981, 1984). The kinetic parameters for the calculation of rate constants and photolysis rates

were specified according to JPL 2011 recommendations (Sander et al., 2011). The model was run in a diurnally varying mode with no transport until the HO_x concentrations were repetitive which means a steady-state was reached. Two model runs are shown: Kinetics 1 which constrains the model using MLS measurements of H_2O, O_3, and temperature to test the HO_x production and loss balance as well as the HO_x partitioning and Kinetics 2 which, in addition, constrains the model using MLS OH measurements to mostly test the HO_x partitioning (Reactions R10, R11 and R12).

As shown in Fig. 12, in the upper mesosphere (pressures smaller than 0.1 hPa), the Kinetics 1 simulations do not reproduce the magnitude of the measured peak, underestimating it by as much as 60 %. On the other hand, Kinetics 2 shows an improvement in the modeling of this peak, reducing the underestimation to less than 40 %. These discrepancies coincide with the ones discussed in the previous section strongly suggesting that they are related to the model assumptions rather than to measurement errors. As with the SD-WACCM simulations, several factors could be the reason for this discrepancy: it might be due to limitations in our current understanding of middle atmospheric chemistry and/or due to the deficiencies in the model solar spectral irradiance used, in this case Rottman (1982).

Also, considering that Kinetics 2 (the run testing the HO_x partitioning) represents the measured HO_2 better, these simulations might suggest that, the modeling problems are related to the HO_x production and loss balance rather than the HO_x partitioning. In the upper stratosphere and lower mesosphere (between 1 and 0.1 hPa) for the most part the photochemical model underpredicts HO_2 by around 20% concurring with the SD-WACCM simulations as well as with previous studies (Sandor et al., 1998; Khosravi et al., 2013) but contradicting the result of the study by Canty et al. (2006).

5 Summary

We have introduced a stratospheric and mesospheric HO_2 dataset derived from the Aura MLS using an offline retrieval algorithm. This offline HO_2 dataset has three distinct

improvements upon the standard MLS HO_2: (1) an extended pressure range, allowing measurements of the mesospheric peak local maxima that occur at around 0.02 hPa at most latitudes, (2) an extended latitudinal coverage, which allows to measure the poles, where the HO_2 maximum lies, and (3) nighttime HO_2 estimates.

The offline retrieval uses zonal mean MLS radiance spectra divided into daytime (SZA $\geq 90°$) and nighttime (SZA $\leq 100°$) which are then inverted using the optimal estimation technique to produce daily zonal mean HO_2 profiles from 10 to 0.0032 hPa during daytime and from 1 to 0.0032 hPa during nighttime. The vertical resolution of this dataset is about 4 km between 10 and 0.1 hPa, 8 km at 0.02 hPa, and around 14 km for smaller pressures. Daily precision ranges from 0.1 ppbv in the upper stratosphere to up to 8 ppbv in the upper mesosphere, dropping to ~ 1.4 ppbv and ~ 0.5 ppbv for monthly and yearly averages, respectively. Between 10 and 0.1 hPa, for both daytime and nighttime cases, the total systematic error is around 0.04 ppbv (up to $\sim 10 \times 10^6$ molec cm^{-3}), while for smaller pressure levels the systematic error is as big as 1.2 ppbv ($\sim 0.2 \times 10^6$ molec cm^{-3}).

Comparison with the balloon-borne FIRS-2 measurements revealed that both datasets agree within their uncertainties, however there seems to be an offset with MLS on the low side. Comparisons with SMILES were found to agree both in structure and magnitude within the uncertainties below 0.02 hPa. Qualitatively, the offline MLS HO_2 agrees well with the SD-WACCM model. Quantitatively, however, the offline MLS HO_2 exceeds the model by up to 100 % in the mesosphere during day (in regions where SD-WACCM estimates near zero values) and up to 40 % at night. Also, between 1 and 0.1 hPa, SD-WACCM underpredicts HO_2 by about 20–30% agreeing with previous studies (Sandor et al., 1998; Khosravi et al., 2013) but contradicting the result of the study by Canty et al. (2006).

Using the Caltech/JPL-Kinetics 1-D photochemical model we found similar results. In the upper mesosphere, we found an underestimation by the model by as much as 60 %, and in the upper stratosphere / lower mesosphere an underestimation by about

20%. These results strongly suggest that these discrepancies are related to the model assumptions rather than to measurement errors.

The results presented in this study show that this new dataset, in addition to the standard MLS OH, H_2O, and O_3 measurements, offers the possibility to study the impact of the HO_x family upon the mesospheric O_3 as well as the HO_x dilemma. Furthermore, this retrieval, or a similar one using geomagnetic latitudes to sort the radiances, may help to understand the impact of solar proton events and energetic electron particles upon the HO_x family by comparing averages of days impacted by these events with averages of non-impacted days.

Acknowledgements. We thank M. Allen and K. Willacy for their help with setting up and running the Caltech/JPL-Kinetics 1-D photochemical model. FIRS-2 data was funded by the NASA's Upper Atmosphere Research program. JEM/SMILES mission is a joint project of Japan Aerospace Exploration Agency (JAXA) and National Institute of Information and Communications Technology (NICT). The WACCM modeling work was sponsored by the National Science Foundation and by the NASA Atmospheric Composition: Modeling and Analysis, solicitation NNH10ZDA001N-ACMAP. The research described in this paper was carried out by the Jet Propulsion Laboratory, California Institute of Technology, under contract with the National Aeronautics and Space Administration.

References

Allen, M., Yung, Y., and Waters, J.: Vertical transport and photochemistry in the terrestrial mesosphere and lower thermosphere (50–120 km), J. Geophys. Res., 86, 3617–3627, 1981.

Allen, M., Lunine, J., and Yung, Y.: The vertical distribution of ozone in the mesosphere and lower thermosphere, J. Geophys. Res., 89, 4841–4872, 1984.

Baron, P., Dupuy, E., Urban, J., Murtagh, D. P., Eriksson, P., and Kasai, Y.: HO_2 measurements in the stratosphere and the mesosphere from the sub-millimetre limb sounder Odin/SMR, Int. J. Remote. Sens., 30, 4195–4208, 2009.

Baron, P., Urban, J., Sagawa, H., Möller, J., Murtagh, D. P., Mendrok, J., Dupuy, E., Sato, T. O., Ochiai, S., Suzuki, K., Manabe, T., Nishibori, T., Kikuchi, K., Sato, R., Takayanagi, M., Mu-

rayama, Y., Shiotani, M., and Kasai, Y.: The Level 2 research product algorithms for the Superconducting Submillimeter-Wave Limb-Emission Sounder (SMILES), Atmos. Meas. Tech., 4, 2105–2124, doi:10.5194/amt-4-2105-2011, 2011.

Brasseur, G. P. and Solomon, S.: Aeronomy of the Middle Atmosphere, Chemistry and Physics of the Stratosphere and Mesosphere, 3rd revised and enlarged edn., Springer, the Netherlands, 2005.

Canty, T., Pickett, H. M., Salawitch, R. J., Jucks, K. W., Traub, W. A., and Waters, J. W.: Stratospheric and mesospheric HO_x: results from Aura MLS and FIRS-2, Geophys. Res. Lett., 33, L12802, doi:10.1029/2006GL025964, 2006.

Crutzen, P. J. and Schmailzl, U.: Chemical budgets of the stratosphere, Planet. Space. Sci., 31, 1009–1032, doi:10.1016/0032-0633(83)90092-2 1983.

Eluszkiewicz, J. and Allen, M.: A global analysis of the ozone deficit in the upper stratosphere and lower mesosphere, J. Geophys. Res., 98, 1069, doi:10.1029/92JD01912, 1993.

Ermolli, I., Matthes, K., Dudok de Wit, T., Krivova, N. A., Tourpali, K., Weber, M., Unruh, Y. C., Gray, L., Langematz, U., Pilewskie, P., Rozanov, E., Schmutz, W., Shapiro, A., Solanki, S. K., and Woods, T. N.: Recent variability of the solar spectral irradiance and its impact on climate modelling, Atmos. Chem. Phys., 13, 3945-3977, doi:10.5194/acp-13-3945-2013, 2013.

Farman, J. C., Gardiner, B. G., and Shanklin, J. D.: Large losses of total ozone in Antartica reveal seasonal ClO_x/NO_x interaction, Nature, 315, 2007–2010, 1985.

Garcia, R. R., Marsh, D., Kinninson, D. E., Boville, B., and Sassi, F.: Simulations of secular trends in the middle atmosphere, J. Geophys. Res., 112, D09301, doi:10.1029/2006JD007485, 2007.

Garcia, R. R., López-Puertas M., Funke D., Marsh D. R., Kinnison D. E., Smith A. K., and González-Galindo F.:, On the distribution of CO2 and CO in the mesosphere and lower thermosphere, J. Geophys. Res., 119, 5700–5718, doi:10.1002/2013JD021208, 2014.

Haigh, J. D, Winning, A. R., Toumi, R., and Harder, J. W.: An influence of solar spectral variations on radiative forcing of climate, Nature, 467, 696–699, doi:10.1038/nature09426, 2010

Harder, J. W., Thuillier, G., Richard, E. C., Brown, S. W., Lykke, K. R., Snow, M., McClintock, W. E., Fontenla, J. M., Woods, T. N., Pilewskie, P.: The SORCE SIM solar spectrum: comparison with recent observations, Sol. Phys., 263, 3–24, doi:10.1007/s11207-010-9555-y, 2010.

Jarnot, R. F., Perun, V. S., and Schwartz, M. J.: Radiometric and spectral performance and calibration of the GHz bands of EOS MLS, IEEE T. Geosci. Remote., 44, 1131–1143, 2006.

Johnson, D. G., Orphal, J., Toon, G. C., Chance, K. V., Traub, W. A., Jucks, K. W., Guelachvili, G., and Morillon-Chapey, M.: Measurements of chlorine nitrate in the stratosphere using the ν_4 and ν_5 bands, Geophys. Res. Lett., 23, 1745–1748, 1996.

Jucks, K. W., Johnson, D. G., Chance, K. V., and Traub, W. A.: Observations of OH, HO_2, H_2O and O_3 in the upper stratosphere: implications for HO_x photochemistry, Geophys. Res. Lett., 25, 3935–3938, 1998.

Khosravi, M., Baron, P., Urban, J., Froidevaux, L., Jonsson, A. I., Kasai, Y., Kuribayashi, K., Mitsuda, C., Murtagh, D. P., Sagawa, H., Santee, M. L., Sato, T. O., Shiotani, M., Suzuki, M., von Clarmann, T., Walker, K. A., and Wang, S.: Diurnal variation of stratospheric and lower mesospheric HOCl, ClO and HO_2 at the equator: comparison of 1-D model calculations with measurements by satellite instruments, Atmos. Chem. Phys., 13, 7587–7606, doi:10.5194/acp-13-7587-2013, 2013.

Kikuchi, K., Nishibori, T., Ochiai, S., Ozeki, H., Irimajiri, Y., Kasai, Y., Koike, M., Manabe, T., Mizukoshi, K., Murayama, Y., Nagahama, T., Sano, T., Sano, R., Seta, M., Takahashi, C., Takayanagi, M., Masuko, H., Inatani, J., Susuki, M., and Shiotani, M.: Overview and early results of the Superconducting Submillimeter Wave Limb Emission Sounder (SMILES), J. Geophys. Res., 115, D23306, doi:10.1029/2010JD014379, 2010.

Kinnison, D. E., Brasseur, G. P., Walters, S., Garcia, R. R., Marsh, D. R., Sassi, F., Harvey, V. L., Randall, C. E., Emmons, L., Lamarque, J. F., Hess, P., Orlando, J. J., Tie, X. X., Randel, W., Pan, L. L., Gettelman, A., Granier, C., Diehl, T., Niemeier, U., and Simmons, A. J.: Sensitivity of chemical tracers to meteorological parameters in the MOZART-3 chemical transport model, J. Geophys. Res., 112, D20302, doi:10.1029/2006JD007879, 2007.

Kuribayashi, K., Sagawa, H., Lehmann, R., Sato, T. O., and Kasai, Y.: Direct estimation of the rate constant of the reaction $ClO + HO_2 \rightarrow HOCl + O_2$ from SMILES atmospheric observations, Atmos. Chem. Phys., 14, 255–266, doi:10.5194/acp-14-255-2014, 2014.

Lamarque, J.-F., Emmons, L. K., Hess, P. G., Kinnison, D. E., Tilmes, S., Vitt, F., Heald, C. L., Holland, E. A., Lauritzen, P. H., Neu, J., Orlando, J. J., Rasch, P. J., and Tyndall, G. K.: CAM-chem: description and evaluation of interactive atmospheric chemistry in the Community Earth System Model, Geosci. Model Dev., 5, 369–411, doi:10.5194/gmd-5-369-2012, 2012.

Lean, J., G. Rottman, J. Harder, and G. Kopp: SORCE contributions to new understanding of global change and solar variability. Sol. Phys., 230, 27–53, 2005.

Livesey, N., Snyder, W. V., Read, W. G., and Wagner, P.: Retrieval algorithms for the EOS Microwave Limb Sounder (MLS), IEEE T. Geosci. Remote., 44, 1144–1155, 2006a.

Livesey, N., Kovalenko L., Salawitch, R., MacKenzie, I., Chipperfield, M., Read, W., Jarnot, R., and Waters, J.: EOS microwave limb sounder observations of upper stratospheric BrO: implications for total bromine, Geophys. Res. Lett., 33, L20817, doi:10.1029/2006GL026930, 2006b.

Livesey, N., Read, W. G., Frovideaux, L., Lambert, A., Manney, G. L., Pumphrey, H. C., Santee, M. L., Schwartz, M. J., Wang, S., Cofield, R. E., Cuddy, D. T., Fuller, R. A., Jarnot, R. F., Jiang, J. H., Knosp, B. W., Stek, P. C., Wagner, P. A., and Wu, D. L.: Earth Observing System (EOS) Aura Microwave Limb Sounder (MLS) Version 3.3 Level 2 data quality and description document, JPL D-33509, JPL publication, USA, 2011.

Marsh D. R., Mills M. J., Kinnison D. E., Lamarque J.-F., Calvo N., and Polvani L. M.: Climate Change from 1850 to 2005 Simulated in CESM1(WACCM). J. Climate, 26, 7372–7391, 2013

Merkel, A. W., Harder J. W., Marsh D. R., Smith A. K., Fontenla J. M., and Woods T. N.: The impact of solar spectral irradiance variability on middle atmospheric ozone, Geophys. Res. Lett., 38, L13802, doi:10.1029/2011GL047561, 2011.

Miller, R. L., Suits, A. G., Houston, P. L., Toumi, R., Mack, J. A., and Wodtke, J. A.: The "Ozone Deficit" Problem: $O_2(X, \nu \geq 26) + O(^3P)$ from 226-nm Ozone Photodissociation, Science, 265, 1831–1837, 1994.

Millán, L., Livesey, N., Read, W., Froidevaux, L., Kinnison, D., Harwood, R., MacKenzie, I. A., and Chipperfield, M. P.: New Aura Microwave Limb Sounder observations of BrO and implications for Br_y, Atmos. Meas. Tech., 5, 1741–1751, doi:10.5194/amt-5-1741-2012, 2012

Ochiai, S., Kikuchi, K., Nishibori, T., Manabe, T., Ozeki, H., Mizobuchi, S., and Irimajiri, Y.: Receiver performance of the superconducting submillimeter-wave limb-emission sounder (SMILES) on the international space station, IEEE T. Geosci. Remote., 51, 3791–3801, doi:10.1109/TGRS.2012.2227758, 2013

Pickett, H. M., Read, W. G., Lee, K. K., and Lung, Y. L.: Observation of night OH in the mesosphere, Geophys. Res. Lett., 33, L19808, doi:10.1029/2006GL026910, 2006.

Pickett, H. M., Drouin, B. J., Canty, T., Salawitch, R. J., Fuller, R. A., Perun, V. S., Livesey, N. J., Waters, J. W., Stachnik, R. A., Sander, S. P., Traub, W. A., Jucks, K. W., and Minschwaner, K.: Validation of Aura Microwave Limb Sounder OH and HO_2 measurements, J. Geophys. Res., 113, D16S30, doi:10.1029/2007JD008775, 2008.

Read, W., Lambert, A., Bacmeister, J., Cofield, R. E., Christensen, L. E., Cuddy, D. T., Daffer, W. H., Drouin, B. J., Fetzer, E., Froidevaux, L., Fuller, R., Herman, R., Jarnot, R. F., Jiang, J. H., Jiang, Y. B., Kelly, K., Knosp, B. W., Kovalenko, L. J., Livesey, N. J., Liu, H.-

C., Manney, G. L., Pickett, H. M., Pumphrey, H. C., Rosenlof, K. H., Sabounchi, X., Santee, M. L., Schwartz, M. J., Snyder, W. V., Stek, P. C., Su, H. S., Takacs, L. L., Thurstans, R. P., Vömel, H., Wagner, P. A., Waters, J. W., Webster, C. R., Weinstock, E. M., and Wu, D. L.: Aura microwave limb sounder upper tropospheric and lower stratospheric H_2O and relative humidity with respect to ice validation, J. Geophys. Res., 112, D24S35, doi:10.1029/2007JD008752, 2007.

Rodgers, C.: Inverse Methods for Atmospheric Sounding: Theory and Practice, Vol. 2 of Series on Atmospheric, Oceanic and Planetary Physics, World Scientific, Singapore, 2000.

Rottman, G. J., Barth, C. A., Thomas, R. J., Mount, G. H., Lawrence, G. M., Rusch, D. W., Sanders, R. W., Thomas, G. E., London, J.:, Solar spectral irradiance, 120 to 190nm, October 13, 1981 - January 3, 1982. Geophysical Research Letters, 9: 587–590. doi: 10.1029/GL009i005p00587, 1982.

Sander, S. P., Friedl, R. R., Barker, J. R., Golden, D. M., Burkholder, J. B., Kolb, C. E., Kurylo, M. J., Moortgat, G. K., Wine, P. H., Abbatt, J. P. D., Huie, R. E., and Orkin, V. L.: Chemical kinetics and photochemical data for use in atmospheric studies, Tech. rep., JPL, evaluation number 17, JPL Publ., 10–6, JPL publication, USA, 2011.

Sandor, B. J. and Clancy, R. T.: Mesospheric HO_x chemistry from diurnal microwave observations of HO_2, O_3 and H_2O, J. Geophys. Res., 103, 13337–13351, 1998.

Smith, A. K., Garcia R. R., Marsh D. R., and Richter J. H.:, WACCM simulations of the mean circulation and trace species transport in the winter mesosphere, J. Geophys. Res., 116, D20115, doi:10.1029/2011JD016083, 2011.

Smith, A. K.: Global Dynamics of the MLT, Surv. Geophys. 33, 1177–1230 DOI 10.1007/s10712-012-9196-9, 2012.

Snow, M., McClintock, W. E., Rottman, G., Woods, T. N.: Solar–stellar irradiance comparison experiment II (Solstice II): examination of the solar–stellar comparison technique, Sol. Phys., 230, 295–324, doi:10.1007/s11207-005-8763-3, 2005

Solomon, S., Rusch, D. W., Thomas, R. J., and Eckman, R. S.: Comparison of mesospheric ozone abundances measured by the Solar Mesosphere Explorer and model calculations, Geophys. Res. Lett., 10, 249, doi:10.1029/GL010i004p00249, 1983.

Siskind, D. E., M. H. Stevens, C. R. Englert, and M. G. Mlynczak (2013), Comparison of a photochemical model with observations of mesospheric hydroxyl and ozone, J. Geophys. Res., 118, 195–207, doi:10.1029/2012JD017971

Summers, M. E., Conway, R. R., Siskind, D. E., Stevens, M. H., Offerman, D., Riese, M., Preusse, P., Strobel, D. F., and Russell, III J. M.: Implications of satellite OH observations for middle atmospheric H_2O and ozone, Science, 227, 1967–1970, 1997.

Tikhonov, S.: On the solution of incorrectly stated problems and a method of a regularization, Dokl. Acad. Nauk. SSSR, 151, 501–504, 1963.

Twomey, S.: On the numerical solution of Fredholm integral equation of the first kind by the inversion of linear system produced by quadrature, J. Assoc. Comput. Mach, 10, 97, 1963.

Varandas, A. J. C.: Are vibrationally excited molecules a clue for the "O_3 deficit problem" and "HO_x dilemma" in the middle atmosphere?, J. Phys. Chem. A, 108, 758–769, 2004.

Wang, S., Li, K.-F., Pongetti, T. J., Sander, S. P., Yung, Y. L., Liang, M.-C., Livesey, N., Santee, M., Harder, J., Snow, M., and Mills, F.: Midlatitude atmospheric OH response to the most recent 11-y solar cycle, P. Natl. Acad. Sci. USA, 110, 2023–2028, doi:10.1073/pnas.1117790110, 2013

Waters, J., Read, W., Froidevaux, L., Jarnot, R., Cofield, R., Flower, D., Lau, G., Pickett, H., Santee, M., Wu, D., Boyles, M., Burke, J., Lay, R., Loo, M., Livesey, N., Lungu, T., Manney, G., Nakamura, L., Perun, V., Ridenoure, B., Shippony, Z., Siegel, P., Thurstans, R., Harwood, R., and Filipiak, M.: The UARS and EOS microwave limb sounder experiments, J. Atmos. Sci., 56, 194–218, 1999.

Waters, J., Froidevaux, L., Harwood, R., Jarnot, R., Pickett, H., Read, W., Siegel, P., Cofield, R., Filipiak, M., Flower, D., Holden, J., Lau, G., Livesey, N., Manney, G., Pumphrey, H., Santee, M., Wu, D., Cuddy, D., Lay, R., Loo, M., Perun, V., Schwartz, M., Stek, P., Thurstans, R., Boyles, M., Chandra, S., Chavez, M., Chen, G.-S., Chudasama, B., Dodge, R., Fuller, R., Girard, M., Jiang, J., Jiang, Y., Knosp, B., LaBelle, R., Lam, J., Lee, K., Miller, D., Oswald, J., Patel, N., Pukala, D., Quintero, O., Scaff, D., Snyder, W., Tope, M., Wagner, P., and Walch, M.: The Earth Observing System Microwave Limb Sounder (EOS MLS) on the Aura satellite, IEEE T. Geosci. Remote., 44, 5, doi:10.1109/TGRS.2006.873771, 2006.

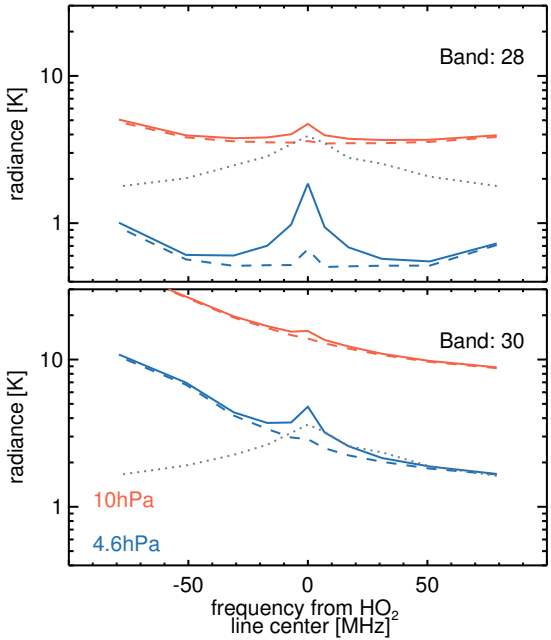

Fig. 1. Average MLS radiance as detected by bands 28 (top) and 30 (bottom), separated into day (solid line) and night (dashed line) time measurements. Average is from 55° S and 55° N and for limb tangents at 10 and 4.6 hPa for January 2005. The dotted gray line is the expected single scan noise.

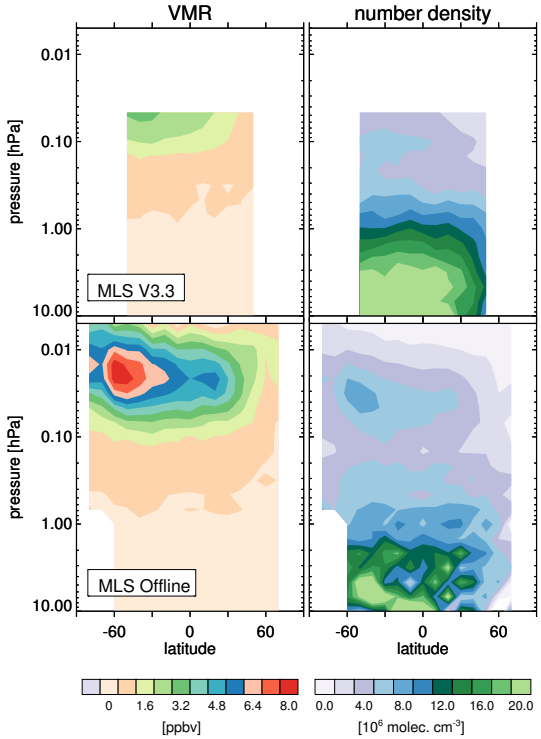

Fig. 2. January 2005 zonal mean for MLS HO_2 datasets. The MLS V3.3 dataset (top) is the standard product described by Pickett et al. (2008), here shown as the day–night difference as recommended by the MLS data guidelines (Livesey et al., 2011). The MLS offline (bottom) is the dataset introduced here. In this case, the day–night difference has been taken only between 10 and 1 hPa, which is the reason why this dataset can be extended to 10 hPa. The left column shows the data in VMR and the right one in number density.

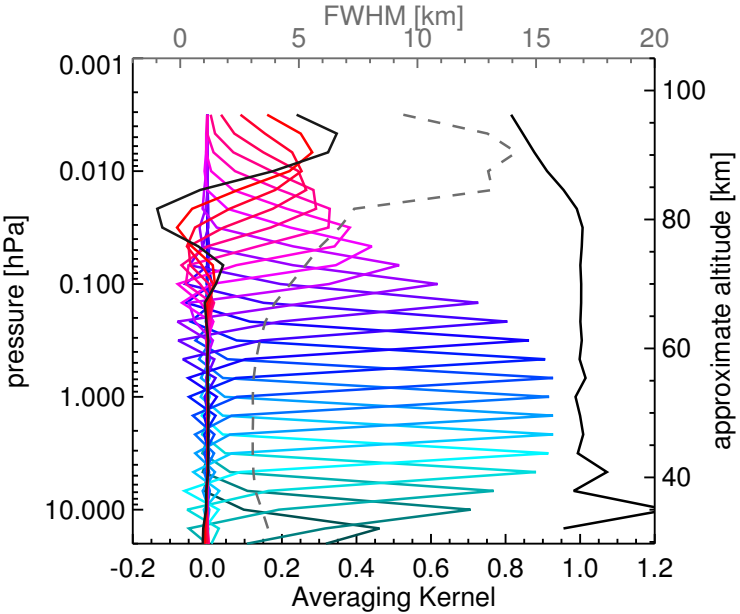

Fig. 3. Daytime averaging kernels for the HO_2 offline retrieval at the equator (those at other latitudes are very similar). The black line is the integrated area under each kernel: values near unity indicate that most information was provided by the measurements while lower values indicate that the retrieval was influenced by the a priori. The dashed gray line is a measure of the vertical resolution of the retrieved profile (derived from the FWHM of the averaging kernels approximately scaled into kilometers).

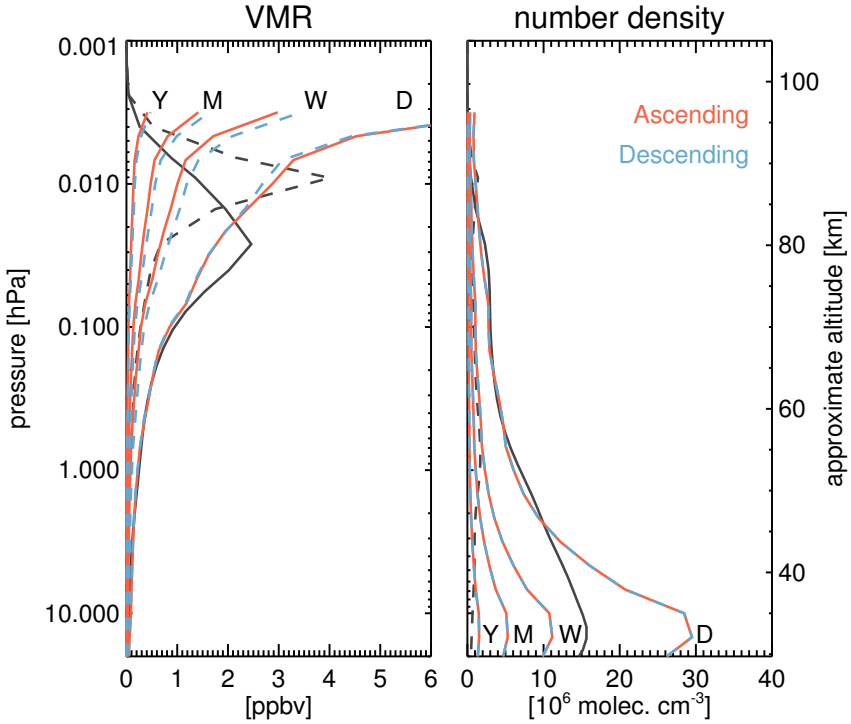

Fig. 4. Precision expected in MLS HO_2 offline data averaged over a 10° latitude bin for a day (D), a week (W), a month (M) and a year (Y). The left column shows the data in VMR and the right one in number density. The black lines show typical HO_2 profiles, daytime in solid and nighttime dashed. These profiles are a yearly average over all latitudes of the SD-WACCM model (see Sect. 4.3 for the model description).

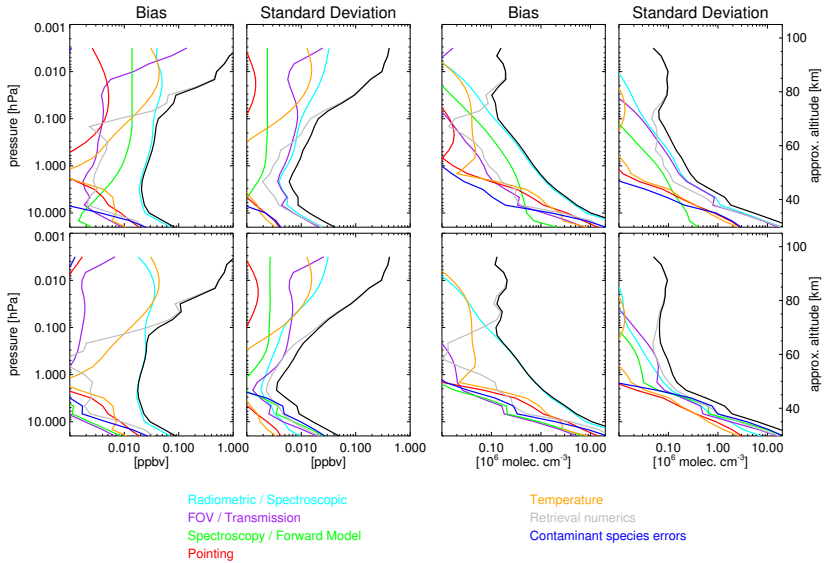

Fig. 5. Estimated impact of various families of systematic error sources on the MLS offline HO_2 observations. Cyan lines correspond to uncertainties in the MLS radiometric and spectral calibration. Purple lines denote uncertainties associated with the MLS FOV and antenna transmission efficiency. Green lines denote errors in the spectroscopic databases and due to the forward model approximations. The impact of the uncertainties in the MLS pointing are depicted by the red lines. The yellow lines correspond to errors in the retrieved MLS temperature, while the blue lines show the impact of the retrieved errors in contaminant species. Errors due to retrieval formulation are shown in gray. The black lines are the root sum squares of all the biases or the scatters shown. The top panel corresponds to the daytime part of the orbit while the lower panel corresponds to the nighttime part. The left panels show the biases and additional scatter introduced by each family of systematic errors in VMR while the right panels show them in number density.

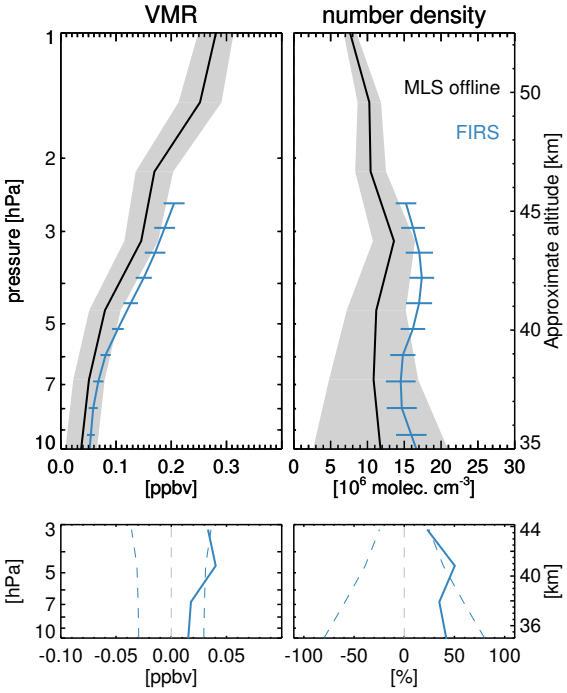
VMR
number density
MLS offline
FIRS
pressure [hPa]
Approximate altitude [km]
[ppbv]
[10^6 molec. cm^-3]
[hPa]
[km]
[ppbv]
[%]

Fig. 6. Comparison of MLS offline and FIRS-2 HO_2 data from 20 September 2005 at 34.5° N. The MLS data correspond to the daytime–nighttime average of the 15 to the 25 September 2005 for the 20° latitude bin centered at 30° N. The FIRS profile corresponds to the one with the closest SZA to the MLS (daytime only) data. The MLS (gray shaded region) and FIRS-2 errors represent a combination of precision and accuracy. The left column shows the data in VMR and the right one in number density. The differences shown in the bottom panels are FIRS-2 − MLS or (FIRS-2 − MLS) 100. / MLS (both in VMR units). The MLS averaging kernels were applied to the FIRS-2 data to fairly compare the two. The errors margins (dashed lines) in the difference subplots correspond to the MLS and FIRS-2 errors added in quadrature.

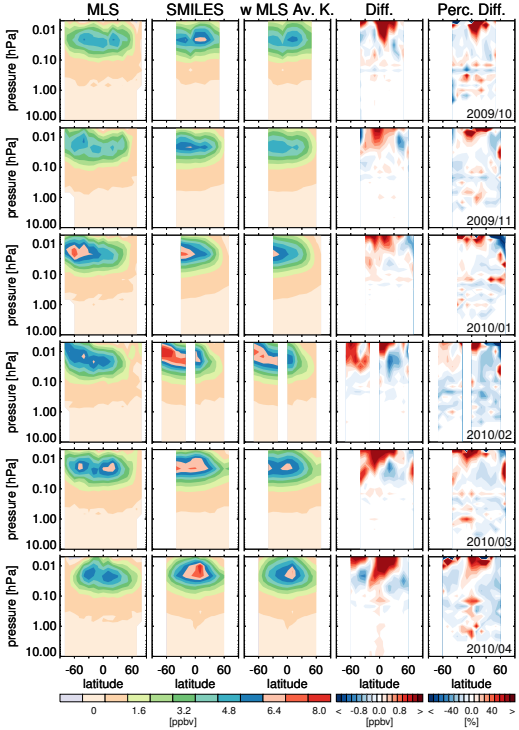

Fig. 7. Monthly daytime zonal mean comparisons between MLS offline and SMILES HO_2 data for October 2009 to April 2011. The MLS averaging kernels were applied to the SMILES data to fairly compare the two. The differences shown are SMILES − MLS or (SMILES − MLS) 100. / MLS (both in VMR units). Note that there is no HO_2 SMILES data available for December 2009. As before, to alleviate biases in the MLS HO_2 data, the daytime–nighttime differences are used as a measure of daytime HO_2 for pressures between 10 and 1 hPa. From left to right, the datasets shown are: MLS, SMILES, SMILES with the MLS average kernels, the absolute difference and the percentage difference.

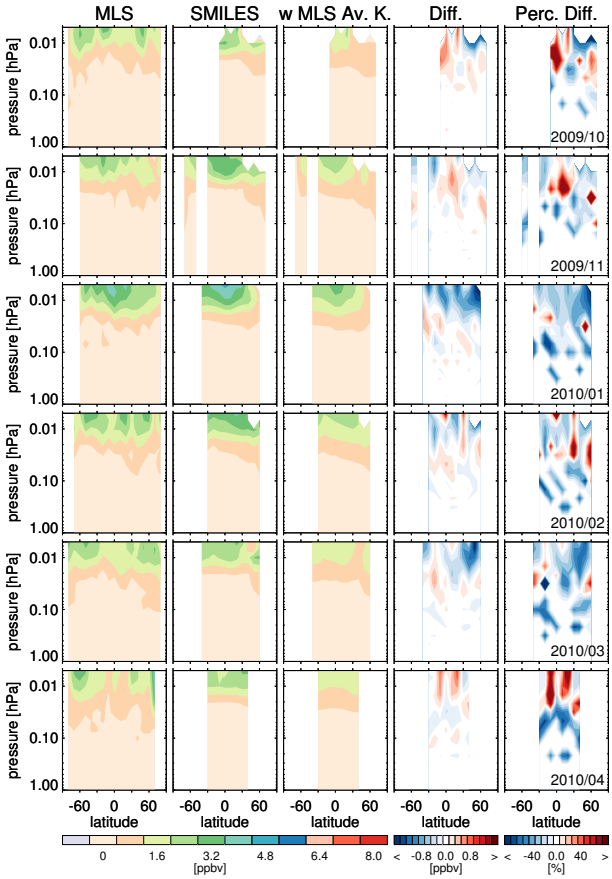

Fig. 8. As for Fig. 7 but for nighttime data. Note that the large positive percentage differences shown for April 2014 close to 20° S and 20° N are due to underestimations by the MLS retrieval.

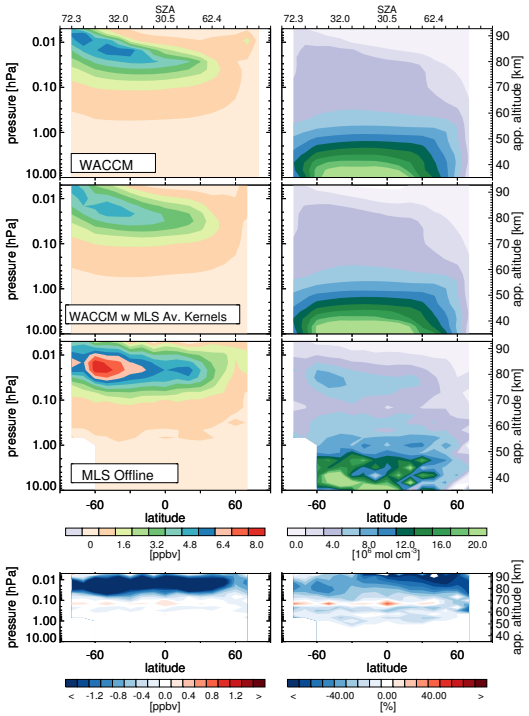

Fig. 9. January 2005 monthly daytime zonal mean for the MLS offline HO_2 observations and the SD-WACCM model. To alleviate biases in the MLS HO_2 data, the daytime–nighttime differences are used as a measure of daytime HO_2 for pressures between 10 and 1 hPa. The MLS averaging kernels were applied to the SD-WACCM dataset to fairly compare the two. The left column shows the data in VMR and the right one in number density. From top to bottom, the datasets shown are: SD-WACCM, SD-WACCM with the MLS averaging kernels, MLS and the absolute and percentage differences. The differences shown are SD-WACCM – MLS or (SD-WACCM – MLS) 100. / MLS (both in VMR units).

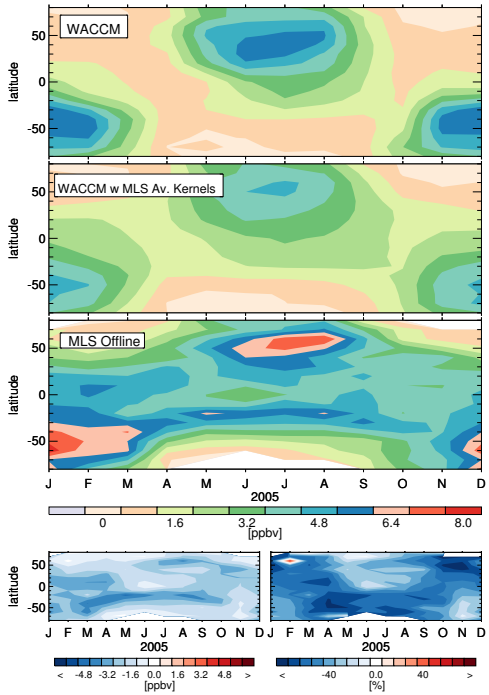

Fig. 10. Daytime latitude/time cross sections of the MLS offline HO_2 observations and the SD-WACCM model for 2005 at 0.014 hPa. As in Fig. 9, the MLS averaging kernels were applied to the SD-WACCM dataset to fairly compare the two. From top to bottom, the datasets shown are: SD-WACCM, SD-WACCM with the MLS averaging kernels, MLS and the absolute and percentage differences. The differences shown are SD-WACCM – MLS or (SD-WACCM – MLS) 100. / MLS (both in VMR units).

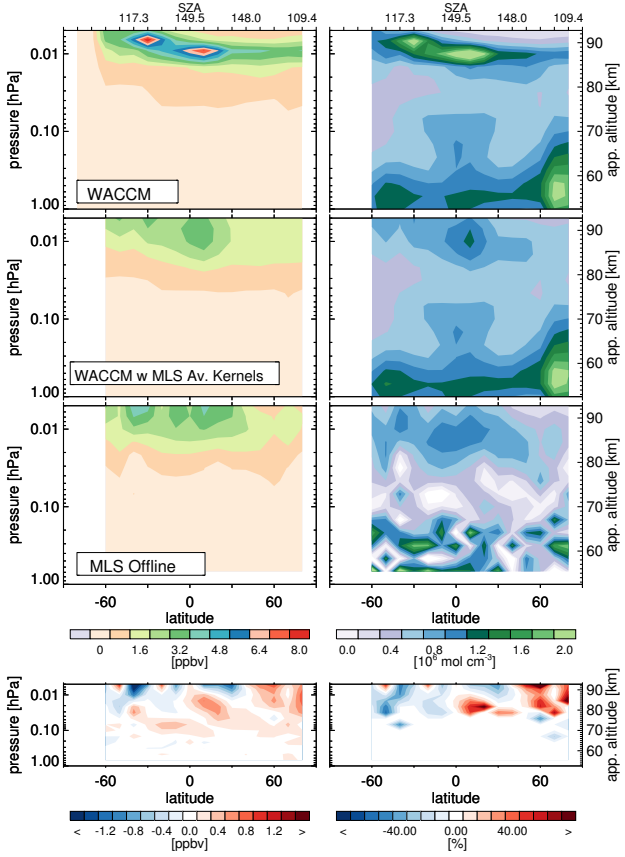

Fig. 11. Same as Fig. 9, except that for nighttime.

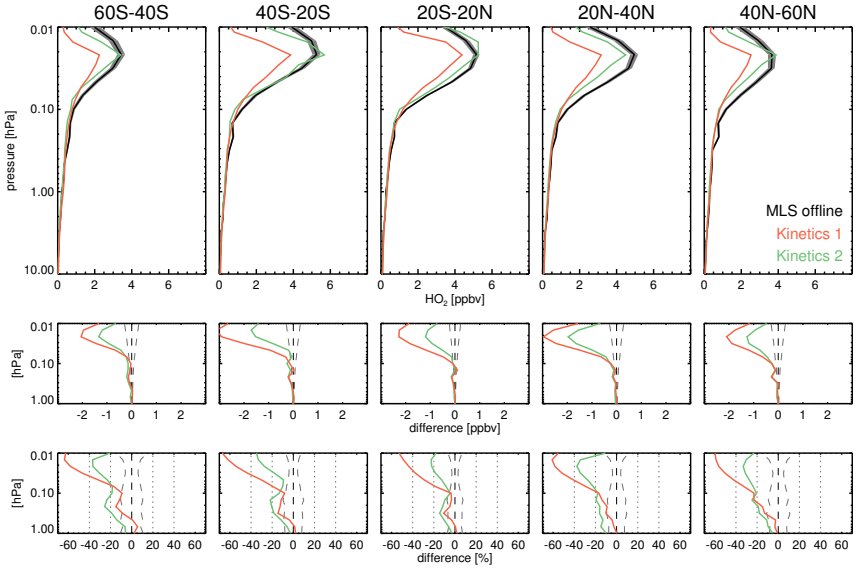

Fig. 12. Daytime MLS offline HO_2 estimates for April 2005 and model results using JPL11 kinetics. Kinetics 1 is a photochemical model run constraining H_2O, O_3, and temperature while Kinetics 2 constrains H_2O, O_3, temperature plus OH. The differences shown are Kinetics − MLS or (Kinetics − MLS) 100. / MLS. In the difference subplots, to properly compare the model runs with MLS, a least square fit has been used to reduce the model resolution and the corresponding averaging kernels has been applied. The dashed gray lines show the MLS precision as well as the 20 and 40% percentage regions.